Ocean Sci. Discuss., 9, 1313–1347, 2012
www.ocean-sci-discuss.net/9/1313/2012/
doi:10.5194/osd-9-1313-2012

Ocean Science Discussions

High Resolution 3-D temperature and salinity fields derived from in situ and satellite observations

S. Guinehut[1], **A.-L. Dhomps**[2], **G. Larnicol**[1], **and P.-Y. Le Traon**[3]

[1]CLS-Space Oceanography Division, Ramonville Saint-Agne, France
[2]LEGOS, Toulouse, France
[3]IFREMER, Plouzané, France

Received: 28 February 2012 – Accepted: 6 March 2012 – Published: 22 March 2012

Correspondence to: S. Guinehut (sguinehut@cls.fr)

Published by Copernicus Publications on behalf of the European Geosciences Union.

Abstract

This paper describes an observation-based approach that combines efficiently the main components of the global ocean observing system using statistical methods. Accurate but sparse in situ temperature and salinity profiles (mainly from Argo for the last 10 years) are merged with the lower accuracy but high-resolution synthetic data derived from altimeter and sea surface temperature satellite observations to provide global 3-D temperature and salinity fields at high temporal and spatial resolution. The first step of the method consists in deriving synthetic temperature fields from altimeter and sea surface temperature observations and salinity fields from altimeter observations through multiple/simple linear regression methods. The second step of the method consists in combining the synthetic fields with in situ temperature and salinity profiles using an optimal interpolation method. Results show the revolution of the Argo observing system. Argo observations now allow a global description of the statistical relationships that exist between surface and subsurface fields needed for step 1 of the method and can constrain the large-scale temperature and mainly salinity fields during step 2 of the method. Compared to the use of climatological estimates, results indicate that up to 50 % of the variance of the temperature fields can be reconstructed from altimeter and sea surface temperature observations and a statistical method. For salinity, only about 20 to 30 % of the signal can be reconstructed from altimeter observations, making the in situ observing system mandatory for salinity estimates. The in situ observations (step 2 of the method) reduce additionally the error by up to 20 % for the temperature field in the mixed layer and the main contribution is for salinity and the near surface layer with an improvement up to 30 %. Compared to estimates derived using in situ observations only, the merged fields provide a better reconstruction of the high resolution temperature and salinity fields. This also holds for the large-scale and low-frequency fields thanks to a better reduction of the aliasing due to the mesoscale variability. Contribution of the merged fields is then illustrated to qualitatively describe the temperature variability patterns for the 1993 to 2009 time period.

OSD

9, 1313–1347, 2012

1 Introduction

With the Global Monitoring for Environment and Security program (GMES) and its Marine Core Service Fast Track program, the European community consolidates past efforts in pre-operational ocean monitoring and forecasting capacity by setting up the MyOcean project (http://www.myocean.eu). This project has developed an integrated system that is based on observations organized as Thematic Assembly Centers (TAC) and on Monitoring and Forecasting Centers (MFC) (Ocean Science, this issue). Whereas TACs are organized by ocean variables (sea level, SST, sea ice, ocean color, in situ temperature and salinity profiles...), the MFCs are organized by regions that cover the European seas (Black, Mediterranean, Baltic and Arctic seas, North West Shelf and the Bay of Biscay) but also the Global Ocean. Two components have been developed as part of the Global Ocean MFC led by the French Operational Oceanography Mercator Océan project: a model/assimilation component and an observation-based one that provides Global Ocean Observation-based Products (GOOP). The later generates global 3-D thermohaline and geostrophic current fields using satellite and in situ measurements.

Despite the impressive increase of the number of temperature and salinity profiles from the Argo array (the 3000 floats target was reached in November 2007; Roemmich et al., 2009), in situ data still strongly undersample the ocean thermohaline variability. Global 3-D thermohaline analysis from in situ observations is only possible at large-scale and low-frequency resolution (see for ex. Roemmich and Gilson, 2009; Von Schuckmann et al., 2009; among others). In contrast, remote-sensing measurements provide synoptic observations of sea level and sea surface temperature (SST) over the world ocean since 1993, but with no direct estimation of the ocean's interior structure. Many studies have used satellite data to complement subsurface observations either at regional or global scales and using different techniques such as multivariate linear regression or gravest empirical modes. These include the works of Fox et al. (2002), Willis et al. (2003), Swart et al. (2010) and Meijers et al. (2011) to name only a few.

OSD
9, 1313–1347, 2012

In order to reconstruct instantaneous temperature (T) and salinity (S) fields at high temporal and spatial resolution, a merging method is developed here to improve a climatological first guess. It combines the accurate but sparse in situ T/S profiles with the high-resolution but less accurate (as synthetic T/S fields) altimeter and SST measurements. This is only possible since, in one hand, sea level anomalies (SLA) from altimeter measurements and dynamic height anomalies (DHA) calculated from in situ T and S profiles are strongly correlated (Gilson et al., 1998; McCarthy et al., 2000; Guinehut et al., 2006; Dhomps et al., 2011), and, in other hand, satellite SST observations can additionally be used to constrain the thermal structure of the ocean in the first hundred meter depth.

The merging method was first developed using simulated data sets (Guinehut et al., 2004) and then using real observations but at regional scale (Larnicol et al., 2006). It has two main steps. The first step consists in deriving synthetic T fields from the surface down to 1500 m depth from altimeter and SST observations through a multiple linear regression method and covariances calculated from historical data. Synthetic S fields are derived in a very similar way but using a simple linear regression method of altimeter observations. The second step consists in combining the synthetic field with in situ T and S profiles using an optimal interpolation method. The global 3-D thermohaline fields are computed in near real time on a 1/3° Mercator horizontal grid, every 7 days (Wednesday only fields) and from the surface down to 1500 m depth on 24 vertical levels. The method has been applied to the 1993 to 2009 time period.

The primary goal of the paper is to demonstrate that the main components of the global ocean observing system can be integrated efficiently using statistical methods. It has two specific objectives. The first one is to provide a global description of statistical relationships that exist between surface and subsurface fields using in situ observations only. The second one is to quantify the capacity of such relationships to be used to reconstruct the interannual variability of the 3-D Ocean thermohaline fields together with additional in situ observations.

OSD
9, 1313–1347, 2012

The paper is organized as follows. All data sets used in the study are presented in Sect. 2. 3-D thermohaline fields computed from satellite observations are then described in Sect. 3. Section 4 presents the combination with the in situ profiles. The interannual variability reconstructed by the thermohaline fields is then analyzed in Sect. 5 before the conclusions.

2 Data

Three sources of ocean observations are used in our study: in situ T and S profiles, satellite altimeter SLA and satellite SST. Each of them is described below. The ARIVO climatology used as first guess for products generation is also described as well as the Scripps monthly gridded fields which are used for an intercomparison exercise.

2.1 In situ T/S profiles

Historical T and S profiles are first used to compute the statistics that relate the surface to subsurface fields. The historical dataset has been constructed using all T and S profiles available in the EN3 dataset (Ingleby and Huddleston, 2007), except those labeled as Argo floats. This historical dataset has then been complemented with the Argo floats observations available at the Coriolis Global Data Acquisition Center as of February 2009 (http://www.coriolis.eu.org). It covers the 1950 to 2008 time period. As this dataset is used to compute the statistics that relate the surface fields (SLA and SST) to subsurface ones, only profiles containing both temperature and salinity (used to calculate a dynamic height) and valid up to 1500 m depth are selected.

T/S profiles from another dataset (CORA3.1) are then used to be combined with the synthetic fields or for validation of the synthetic estimates. It comes from the Coriolis data center which is the MyOcean TAC for in situ observations. It includes Argo floats, XBT, CTD and moorings profiles for the 1993 to 2009 time period (Cabanes et al., 2011).

OSD
9, 1313–1347, 2012

2.2 Gridded maps of altimeter sea level anomalies

The altimeter data used are from the SSALTO/DUACS center which is the MyOcean TAC for satellite sea level observations. They consist in gridded products of SLA obtained from an optimal combination of all available satellite altimeters (AVISO, 2012). The delayed-mode version of the product is used. The maps are available every 7 days (Wednesday only fields) on a 1/3° Mercator grid and the 1993–2009 time series have been used.

2.3 Gridded maps of sea surface temperature observations

Satellite SST data are from daily Reynolds L4 analyses with a 1/4° horizontal resolution, combining AVHRR, AMSR and in situ observations and distributed by the National Climatic Data Center at NOAA (Reynolds et al., 2007). Again, the 1993–2009 time series of the Wednesday fields have been used.

2.4 ARIVO climatology

Temperature and salinity monthly fields from the ARIVO climatology are used to compute anomalies of the T and S profiles from a climatological monthly means (Gaillard and Charraudeau, 2008). The ARIVO climatology has been computed as part of the Mersea European project, the predecessor of the MyOcean project. It is defined on a 1/2° Mercator horizontal grid, for the first 2000 meters on 151 vertical levels and for the global ocean. It has been computed using an optimal interpolation method and all available in situ T and S profiles for the 2002 to 2007 periods. It is thus representative of this period.

2.5 Gridded fields of temperature and salinity from Argo floats

Gridded fields of temperature and salinity from the Scripps Institution of Oceanography are also used as an external solution for validation. Those are monthly fields defined

OSD
9, 1313–1347, 2012

on a 1° horizontal grid from the surface down to 2000 dbar on 58 vertical levels. They are computed using only Argo T and S profiles and an optimal interpolation method (Roemmich and Gilson, 2009). The fields are available in near real-time since January 2004.

3 3-D thermohaline fields from satellite observations

The first step of the method consists in deriving synthetic T and S fields from altimeter and SST observations using a multiple/simple linear regression method and covariances calculated from historical in situ observations. A global description of the statistical relationships that exist between surface and subsurface fields is first performed using in situ observations only (Sect. 3.1). As these statistical relationships are estimated using a dynamic height calculated with a reference level at 1500 m depth for SLA, preprocessing of altimeter measurements is needed to make them consistent with a dynamic height calculated for the first 1500 m depth of the ocean. The methodology is presented below (Sect. 3.2). The method is then validated using independent dataset (Sect. 3.3).

3.1 Relationship between surface and subsurface fields

Synthetic T and S fields are first derived from altimeter and SST observations using a multiple/simple linear regression methods that are expressed as:

$$T(x,y,z,t) = \alpha(x,y,z,t).SLA'(x,y,t) + \beta(x,y,z,t).SST'(x,y,t) + Tc\lim(x,y,z,t) \quad (1)$$

and

$$S(x,y,z,t) = \gamma(x,y,z,t).SLA'(x,y,t) + Sc\lim(x,y,z,t). \quad (2)$$

where SLA′ and SST′ denotes anomalies from the ARIVO monthly climatology (see Sect. 2.4), Tclim and Sclim denotes the ARIVO monthly fields and α, β and γ are

OSD
9, 1313–1347, 2012

the regression coefficients of the SLA and SST onto temperature and of SLA onto salinity. They vary with depth, time and geographical location and are expressed as covariances between the variables (only the z variable is indicated here for clarity):

$$\alpha(z) = \frac{\langle SST', SST' \rangle . \langle SLA', T'(z) \rangle - \langle SLA', SST' \rangle . \langle SST', T'(z) \rangle}{\langle SLA', SLA' \rangle . \langle SST', SST' \rangle - \langle SLA', SST' \rangle^2}, \quad (3)$$

$$\beta(z) = \frac{\langle SLA', SLA' \rangle . \langle SST', T'(z) \rangle - \langle SLA', SST' \rangle . \langle SLA', T'(z) \rangle}{\langle SLA', SLA' \rangle . \langle SST', SST' \rangle - \langle SLA', SST' \rangle^2}, \quad (4)$$

$$\gamma(z) = \frac{\langle S'(z), SLA' \rangle}{\langle SLA', SLA' \rangle}. \quad (5)$$

These covariances are calculated using only in situ observations (the historical dataset described in Sect. 2.1) in order to better describe the relationship that exists for each profile between its surface and subsurface properties. The T observation at the surface is taken for SST and dynamic height (DH) calculated using the measured T and S profiles and a reference level at 1500 m depth is taken for SLA.

Covariances are computed locally on a global 1° horizontal grid using all observations available in a radius of influence around each grid point. This radius of influence is set to 5° in latitude. In longitude, it starts with a 10° value and is increased up to 20° for the annual statistics and up to 25° for the seasonal statistics to match a minimum number of 500 profiles available for the computation of the statistics at each horizontal grid point. The radius of influence is increased in longitude mainly in the tropical Pacific Ocean and in the Southern Ocean (South of 50° S) and to a less extent in the tropical Indian and Atlantic Oceans.

Normalized covariances (i.e. correlation coefficients) between dynamic height (DH) and T at 100 m depth is illustrated on Fig. 1. The horizontal structure of the correlation is large-scale with values higher than 0.6 in most part of the Indian and Pacific Ocean. Away from western boundary regions, the Atlantic Ocean shows lower values of the

OSD
9, 1313–1347, 2012

order of 0.4 to 0.6. Three latitudinal sections, one in each Ocean, have been selected to illustrate the 2-D vertical view of the correlations (Fig. 2).

DH-T(z) correlation coefficients show very similar structures as a function of latitude and depth for all three oceans (Fig. 2). The mid-latitude regions have values greater than 0.6 bellow 100 m and down to 1500 m. In the tropics the maximum correlation is reached at 100 m with values of 0.3 to 0.4 elsewhere. Negative values of the order of −0.2 are visible at depth between 800 and 1500-m around 20° S in the Atlantic Ocean, 10° S in the Indian Ocean and along the Equator in the Pacific Ocean.

DH-S(z) correlation coefficients show also very similar structures as a function of latitude and depth for all three oceans south of 30° N (Fig. 2). The North Atlantic and North Pacific Oceans have indeed very different structures with values very negative and lower than −0.6 for the Pacific Ocean and positive values of the order of 0.3–0.4 in the Atlantic Ocean. In the tropics, the three oceans show negative values from the surface down to 100 m, then positive values down to 600 m in the Atlantic and Pacific Ocean and only down to 200 m in the Indian Ocean. The values are then again negative more deep. DH-T(z) and DH-S(z) show well correlated baroclinic structures in the tropics. All three Southern Oceans show a very negative tong with value of the order of −0.8. This tong is close to 70° S next to the surface and varies from 40° S to 60° S from the Atlantic to the Pacific Oceans. Any small variation of the salinity field in this area will thus have a significant impact on the sea level.

Correlation coefficients between SST and T(z) are also very similar for the three sections but with slight differences (Fig. 2). Values are maximum at all latitudes in the top 20 m. A vertical tong of maximum values (0.5–0.6) is visible for all depths in the three oceans, at 50° S in the Atlantic Ocean, at 45° S in the Indian Ocean and at 55° S in the Pacific Ocean. Most values are elsewhere low and comprised between −0.2 and 0.2.

OSD
9, 1313–1347, 2012

3.2 Pre-processing of altimeter measurements

As discussed previously, the use of the covariances described in the previous section with observed altimeter SLA requires a preprocessing of altimeter observations to make them consistent with a dynamic height calculated for the first 1500 m of the ocean.

The differences between a dynamic height calculated using a reference level at 1500 m and altimeter SLA, assuming measurements errors negligible, represent the circulation at the reference level, or in other words, the deep baroclinic (below 1500 m) and the barotropic components of the circulation. At 1500 m, the circulation is not null and has to be removed from altimeter height before applying the regression. This is obtained here using regression coefficients calculated between Dynamic Height Anomaly (DHA) computed from Argo T/S profiles and a reference level at 1500 m and Sea Level Anomaly (SLA) altimeter collocated measurements. The method is very similar to the one described in Guinehut et al. (2006) and Dhomps et al. (2010) except that the reference level is taken at 1500 m.

The spatial structure of the regression coefficient is largely dependent on latitude (Fig. 4). In the equatorial and tropical regions, the vertical structure of the ocean is mainly baroclinic with regression coefficients between SLA and DHA greater than 0.8. Most part of altimeter SLA signal will thus be projected onto the vertical. At mid to high latitudes, the vertical structure of the ocean is more barotropic with regression coefficient from 0.7 to 0.2 meaning that only 70 to 20 % of the altimeter fields are projected onto the vertical.

Before applying the regression coefficient to each altimeter gridded maps, an additional preprocessing is needed since altimeter observations are given as anomalies from the 1993–1999 periods (AVISO, 2012). These anomalies are thus first recalculated using a 6-year time mean from 2002 to 2006 to be consistent with the ARIVO climatology (Gaillard and Charraudeau, 2008) which is defined for this 6-year time period and which is then used to compute anomalies of SLA from the seasonal cycle.

OSD
9, 1313–1347, 2012

Regression coefficients are then applied to each of the altimeter gridded maps to generate the altimeter data sets that will be used for the vertical projection. These fields are names hereafter "steric" SLA.

3.3 Comparison with independent dataset

The impacts of the pre-processing of the altimeter measurements as well as the impact of the combination of altimeter and SST observations to derive synthetic T and S fields are evaluated using independent dataset. Temperature and salinity synthetic fields are first calculated from SLA, "steric' SLA (i.e. derived from the regression method described in Sect. 3.2) and a combination of "steric" SLA and SST. They are computed on a 1/3° Mercator horizontal grid, every 7 days (Wednesday only fields) and from the surface down to 1500 m on 24 vertical levels. The full 1993 to 2009 time period has been processed. As the historical T and S profiles used to compute the covariances cover the 1950 to 2008 time period, independent in situ T and S profiles of the year 2009 from the CORA3.1 dataset (see Sect. 2.1) are used to validate the synthetic fields of the year 2009.

The impact of the pre-processing of the altimeter measurements is first evaluated by calculating the error in reconstructing subsurface T and S synthetic fields using a simple regression method of total and "steric" SLA and by comparing their quality to climatological estimates. Synthetic and climatological fields from the ARIVO climatology (see Sect. 2.4) are first interpolated at the time and position of each in situ independent T and S profiles. Statistics (mean and rms of the differences) are then calculated from each pairs (in situ and synthetic, in situ and ARIVO). Results are illustrated in the Antarctic Circumpolar Current (ACC) region where the circulation at 1500 m is not negligible (Fig. 4). They show that the pre-processing of the altimeter measurements reduces the rms error by 5 % at almost all depths for the T fields and up to 10 % for the S fields between 800 and 1300 m (compare the black and blue curves on Figs. 5 and 6).

OSD
9, 1313–1347, 2012

For the T field, the additional information provided by satellite SST reduces the rms error at depth up to 900 m with major impact in the surface and mixed layers. Still in the ACC region, rms error is now about 0.5 °C at the surface compared to 0.85 °C when using only altimeter observations and compared to nearly 1 °C when using climatological estimates.

At the global scale, results indicate additionally that the temperature bias that existed for all depths when using the ARIVO climatology fields is reduced when using the synthetic estimates (Fig. 7). Mean errors are almost zero for all depths when using the synthetic fields. Rms error range from 0.5 °C at the surface, with a maximum of 0.9 °C in the mixed layer depth decreasing to 0.15 °C down to 1000 m. Compared to the use of climatological estimates, results indicate that 50 % to 30 % at depth of the temperature fields can be reconstructed from altimeter and SST satellite observations and a statistical method. For salinity, only of about 30 to 20 % of the salinity can be reconstructed from altimeter observations (Fig. 8). Rms error in predicting subsurface salinity from the synthetic fields are very close to the one obtained from the ARIVO fields and range from 0.17 psu at the surface to 0.03 psu at depth.

4 Combination with in situ T/S profiles

The second step of the method consists in combining the synthetic estimates with all available in situ T/S profiles using an optimal interpolation method (Bretherton et al., 1976). The method has first been developed using simulated data (Guinehut et al., 2004) and is now applied to real observations.

4.1 Method

The key issue here is to gain maximum benefits from the qualities of both data sets, namely the accurate information given by the sparse in situ profiles and the mesoscale content provided by the synthetic fields. Le Traon et al., (1998) and Guinehut et

OSD
9, 1313–1347, 2012

al. (2004) have showed that a precise statistical description of the errors on these observations must be introduced in the optimal interpolation method. In addition to the conventional use of a measurement white noise, an a priori bias of 20 % of the signal variance and a spatially correlated error of also 20 % are applied to the synthetic fields to correct large-scale errors and bias introduced by the first step of the method (i.e. the regression method). These values have been estimated empirically and more accurate estimates are left for future studies.

As the main objective of the combination is to correct the large-scale part of the synthetic fields using the surrounding in situ profiles, signal spatial correlation scales are set two times those used to compute the altimeter gridded maps (AVISO, 2012). They vary from 700 km (resp. 500 km) at the equator to 300 km north of 60° N in the zonal (resp. meridional) directions. The temporal correlation scale is fixed at 15 days everywhere. The signal space-time correlation function is the same as the one used in Guinehut et al. (2004). An example of the input and output fields is given on Figure 9 for the 4 July 2007. Thanks to the mesoscale structures available in the altimeter and SST fields, the synthetic estimate shows mesoscale structures in most part of the ocean with T anomalies ranging from −5 to 5 °C at 100 m (Fig. 9c). The combination of the synthetic estimates with all available in situ T allows correcting the field in some regions like in the North-East Indian Ocean where the in situ T are much colder than the synthetic ones, revealing a shallower thermocline. Amplitudes of the combined fields are thus more similar to the in situ observations but still resolving small-scale structures (Fig. 9e). Furthermore, the combined fields allow resolving much smaller-scale structures than the ones obtained by an in situ only field computed using all in situ observations available and an optimal interpolation method (compare Fig. 9e and f).

As the synthetic fields, the combined estimates are computed on a 1/3° Mercator horizontal grid, every 7 days (Wednesday only fields) and from the surface down to 1500 m on 24 vertical levels. The full 1993 to 2009 time period has been processed using the in situ T and S profiles from the CORA3.1 dataset describes in Sect. 2.1. In

OSD
9, 1313–1347, 2012

situ T and S profiles of the year 2009 are also used (as for the synthetic fields (see Sect. 4.2)) to validate the combined fields of the year 2009. As these comparisons are not independent, the objective here is to check the capacity of the combination method to accurately merge the two types of observations. As the in situ observations are used to correct large-scale structure of the synthetic fields, zero differences are not expected.

Results show that the very small residual mean error that was present in the synthetic temperature fields has now disappeared (Fig. 7). Rms error is reduced for all depth but mainly in the 100–300 depth layers where the in situ observations impact mostly to correct the depth of the mixed layer. This is true for the global ocean but major impacts are observed in the tropics (Fig. 9). Residual rms difference with in situ profiles range from 0.3 °C at the surface with a slight maximum of 0.42 °C at 50 m and down to less than 0.1 °C below 1000 m. Results are improved by more than 20 % (to 40 % at depth) compared to the use of synthetic estimates alone. For salinity, as only a small part of the signal can be reconstructed from altimeter observations, the in situ profiles reduce the residual error by more than 40 % for all depths. This result already shows that the in situ observing system and particularly the Argo floats with their global coverage are mandatory for salinity fields estimates.

Independent comparisons (not showed) with a subset of in situ T and S profiles allowed us to estimate more precisely the contribution of the in situ observing system to the 3-D thermohaline fields reconstruction. In situ observations decrease the error in predicting subsurface T by at least 5 % at depth and 20 % in the mixed layer depth and near the surface. The main contribution is for the surface salinity field where the error in predicting near surface S is decreased by 30 %. The gain is also visible at depth with improvement of about 10 %.

4.2 Towards a better restitution of large-scale signals

The merging method developed here improves greatly the climatological first guess and provide a much better estimation of the T and S fields at high temporal and spatial

OSD
9, 1313–1347, 2012

resolution than the one that could be obtained using in situ observations only. Another example is given on Fig. 10 along a cruise performed in June 2008 in the North Atlantic Ocean between Portugal and Greenland as part of the OVIDE project (Lherminier et al., 2007). The in situ only estimate computed using all in situ profiles available nearby the cruise, except those taken during the cruise allow the reconstruction of the very large-scale structure along the section. The mesoscale structures present in the satellite fields (altimeter and SST) allow a much better reconstruction of the mesoscale structures but with a smoother shape (synthetic and combined fields).

Nevertheless, as already demonstrated using simulated observations (Guinehut et al., 2004), the reduction of the aliasing due to the mesoscale variability should be instrumental in reconstructing the large-scale and low-frequency part of the fields. This has been verified using four realizations of the OVIDE cruise (years 2002, 2004, 2006 and 2008). For each of the cruises, the in situ T and S section are compared to reconstructed fields using only in situ observation and from the combined method. For both estimates the in situ profiles from the cruises are (or course) not used. This is done for the instantaneous fields and also for the large-scale part of the fields (scales larger than 400 km). From the 365 profiles measured during the four OVIDE cruises, and for the T and S fields, the improvement in reconstructing instantaneous fields is about 30 % of the signal variance using the combined estimates compared to an in situ solution and this number increase up to 50 % for the large-scale part of the field. This result is obtained using a small number of in situ independent profiles but it clearly demonstrates that a better reconstruction of the mesoscale structures is required for the reconstruction of the large-scale part of the signal.

5 Interannual variability reconstructed from the 3-D thermohaline fields

The interannual variability reconstructed by the observation-based fields is now studied. Yearly zonal averages of the synthetic and combined fields as anomalies from

OSD
9, 1313–1347, 2012

the 2004 to 2009 periods are first compared to the SCRIPPS independent estimate (Roemmich and Gilson, 2009; see Sect. 2.5).

For the temperature field, results are very similar in terms of amplitude and geographical position for the synthetic, combined and SCRIPPS estimates (Fig. 11). The signals vary from −0.4 to 0.4 °C with very clear and strong year to year baroclinic variability at the equator. These strong signals are confined in the top 200 m and are mainly driven by the successive El Nino/La Nina events. Even if the Pacific Ocean plays a major role in the global mean, the Indian and to a less extent the Atlantic Oceans show also strong baroclinic equatorial variability. At mid to high latitudes, the amplitudes of the signals are smaller (from −0.2 to 0.2 °C) but their structure is vertically coherent down to 1000 m and even deeper between 40 and 50° N in the Atlantic Ocean. Since the year to year variability in the Southern Ocean is not positioned at the same latitude in all three oceans, the global mean shows very low amplitude signals (< 0.05 °C) for the 2004 to 2009 periods. Those signals are very consistent with the one described in von Schuckmann et al. (2009) who provide a global description of large-scale temperature signals for the 2003 to 2008 time period. Satellite observations such as SLA and SST combined with a statistical description of the vertical structure of the ocean are thus able to reconstruct the interannual variability patterns of the 3-D temperature field. There is no bias or spurious signals introduced by the method. The variability of the 1993 to 2000 periods which suffers from poor in situ measurements coverage (see among others Roemmich and Gilson, 2009) could now be studied (see below).

The picture is nevertheless really different for the salinity field since the synthetic estimates are not able at all to reproduce any interannual variability (not showed). This result confirms the fact that the in situ Argo observing system is really mandatory for salinity. For the combined and SCRIPPS estimates, the signals are very similar and vary between −0.05 to 0.05 psu. They show again very clear and strong interannual variability at the equator that is generally correlated to what is observed for temperature. At mid to high latitudes the global mean signals show small scale pattern limited mainly to the first 500 meters. Again, results are very different between the three

OSD
9, 1313–1347, 2012

oceans. The Atlantic Ocean shows deep vertically coherent structures as deep as 1500 meter around 40° N and to 1000 m around 30° S with value of the order of 0.02 psu at depth. The vertical extension of the signals in the Indian and Pacific Oceans are limited to the first 500 mr and their amplitude is also smaller (see also von Schuckmann et al., 2009). Unlike the temperature field, the observation-based method presented here is unfortunately of any help to describe the interannual variability of the salinity field for the years previous Argo.

The temperature variability of the 17-years from 1993 to 2009 can now be qualitatively described using the combined fields. The objective is to illustrate the capacity of the method and further analysis will be needed to understand the observed signal and relate them to some forcing mechanisms. This is left for future studies. Results are again presented as global zonal averages and as anomalies from the full period. Even if results vary between the three Oceans, clear tendencies can be extracted from the global means. As for the 2004 to 2009 periods, the amplitude of the signals varies between −0.4 and 0.4 °C with maximum value up to 1.2 °C. Again strong interannual baroclinic variability is found in the equatorial region with a succession of deepening and outcrop of the main thermocline. A clear long term warming is visible in the Southern Ocean of up to 0.8 °C for the 1993 to 2009 period with a signature down to 1300 m. The warming is not limited to the southern part of the southern ocean but is clearly visible at all latitudes between 50° S and 20° S. Rather than a long term trend, a succession of warming and cooling events is visible further south. The variability of the northern hemisphere is much more complex at the global scale with a succession of warming and cooling events at mid and high latitudes revealing the necessity to study more precisely what is going on separately in the Atlantic and Pacific Oceans.

OSD
9, 1313–1347, 2012

6 Conclusions and perspectives

To understand, monitor and predict the ocean state, Global Ocean Observation-based Products (GOOP) that combines satellite and in situ measurements have been developed. Global instantaneous 3-D thermohaline fields are thus generated on a 1/3° Mercator horizontal grid, every 7 days and from the surface down to 1500 m depth. Near real time products are available and the full 1993 to 2009 time period has been processed. The main contribution of this study is, however, to show that the accurate but sparse in situ T/S profiles observations can be effectively merged with the lower accuracy but high-resolution synthetic data derived from satellite altimeter and sea surface temperature observations. The merging provides a much better estimation of the instantaneous but also large-scale and low-frequency 3-D temperature and salinity fields compared to estimates computed using only in situ observations. It has been showed that the reduction of the aliasing due to the mesoscale variability is a necessary step for the reconstruction of the large-scale and low-frequency part of the fields. This had been demonstrated using simulated observations (Guinehut et al., 2004) and it is confirmed here using real observations.

Hydrographic variability patterns for the temperature field, over the 1993 to 2009 time period and for the global ocean show that most part of the Southern Ocean is dominated by a clear long term warning and that the equatorial region and the Northern Hemisphere are dominated by interannual to decadal variability. The observed signals have been qualitatively described and regional analyses are needed to better understand them and relate them to different forcing mechanisms. This is left for future studies. The description of the temperature variability pattern for the years previous to the Argo era has only been made possible by the statistical relationships between surface and subsurface fields computed using only in situ observations, and mainly Argo profiling floats observations. Argo has then indirectly helped the description of the variability of the 1993 to 2000 time period. It is however much more difficult to infer the vertical structure of the salinity field from satellite SLA observations and a statistical

OSD
9, 1313–1347, 2012

description of the vertical structure of the ocean. This result shows that the in situ observing system and the Argo profiling floats are mandatory for salinity estimates. New satellite missions measuring Sea Surface Salinity (SSS) as SMOS and Aquarius (Font et al., 2010; Reul et al., 2011) should further help in reconstructing subsurface fields from satellite ones.

The observation-based approach developed here provides an improved and more complete estimate of the state of the ocean compared to estimates based on in situ or satellite observations only. It is also very consistent and very complementary to what ocean reanalysis that combines model and observations through an assimilation method give (Stammer et al., 2010). Other reprocessing and reanalysis will be available from the EU MyOcean I and II projects (Ferry et al., 2010; Haines et al., 2012; Storto et al., 2012). The robustness of the different solutions between statistical methods and observations, models and assimilation systems should be further studied to learn more about the contribution of the different observing systems (Oke et al., 2009, 2010), the physics of the model and the impact of the forcing fields (Garric et al., 2012) and of the assimilation system. This is a necessary step for Ocean Climate Monitoring studies.

Only thermohaline fields are presented here but the Global Ocean Observation-based Products also include 3-D geostrophic velocity estimates that are calculated using the thermal wind equation combined to absolute surface altimeter geostrophic currents (Mulet et al., 2012). First attempts to compute vertical velocities from our observation-based products are performed as part of the EU MyOcean MESCLA R&D project (Buongiorno Nardelli et al., 2012) and open new era for Ocean Climate Monitoring studies, including vertical exchanges associated with mesoscale activity and their relation to biological processes. The present work is a first step toward integrating climate-relevant global ocean datasets such as in situ temperature and salinity profiles and satellite altimeter and sea surface temperature and will be continued towards the restitution of higher resolution products.

OSD
9, 1313–1347, 2012

Acknowledgements. This work was carried out in the framework of the MyOcean project (Development and pre-operational validation of GMES Marine Core Services (2009–2012)) and has been funded within the call EU FP7-SPACE-2007-1 (Grant Agreement nr. 218812) and with support from CNES under contract 82394/00.

References

Antonov, J. I., Seidov, D., Boyer, T. P., Locarnini, R. A., Mishonov, A. V., Garcia, H. E., Baranova, O. K., Zweng, M. M., and Johnson, D. R.: World Ocean Atlas 2009, Volume 2: Salinity. S. Levitus, Ed. NOAA Atlas NESDIS 69, U.S. Government Printing Office, Washington, D.C., 184 pp., 2010.

AVISO: SSALTO/DUACS User Handbook: (M)SLA and (M)ADT near-real time and delayed time products, SALP-MU-P-EA- 21065-CLS, ed. 2.9, 73 pp., 2012.

Buongiorno Nardelli, B., Pascual, A., Guinehut, S., Ruiz, S., and Drillet, Y.: Towards high resolution mapping of 3-D mesoscale dynamics from observations preliminary comparison of retrieval techniques and models with MESCLA project, Ocean Sci. Discuss., 9, 1045–1083, doi:10.5194/osd-9-1045-2012, 2012.

Bretherton, F. P., Davis, R. E., and Fandry, C. B.: A technique for objective analysis and design of oceanographic experiments applied to MODE-73, Deep-Sea Res., 23, 559–582, 1976.

Cabanes, C., Grouazel, A., Coatanoan, C., and Turpin, V.: Coriolis Ocean database for ReAnalysis – CORA3 Documentation, ed. 1.0, 50 pp., (http://www.coriolis.eu.org/Science/Data-and-Products/CORA-Documentation), 2011.

Dhomps, A. -L., Guinehut, S., Le Traon, P.-Y., and Larnicol, G.: A global comparison of Argo and satellite altimetry observations, Ocean Sci., 7, 175–183, doi:10.5194/os-7-175-2011, 2011.

Ferry, N., Parent, L., Garric, G., Barnier, B., Jourdain, N. C., and the Mercator Océan team: Mercator Global Eddy Permitting Ocean Reanalysis GLORYS1V1: Description and Results, Mercator Ocean Quarterly Newsletter #36, January 2010, 15–27, 2010.

Font, J., Camps, A., Borges, A., Martín-Neira, M., Boutin, J., Reul, N., Kerr, Y. H., Hahne, A., and Mecklenburg, S.: SMOS: The Challenging Sea Surface Salinity Measurement from Space, Proc. IEEE, 98, 5, 649–665, 2010.

OSD

9, 1313–1347, 2012

Fox, D. N., Teague, W. J., Barron, C. N., Carnes, M. R., and Lee, C. M.: The Modula Ocean Data Assimilation System (MODAS), J. Atmos. Oceanic Technol.,19, 240-252, 2002.
Gaillard, F. and Charraudeau, R.: New climatology and statistics over the global Ocean, MERSEA-WP05-CNRS-STR- 001-1A, 2008.
Garric, G., Verbrugge, N., and Bricaud, C.: Large scale ERA-Interim radiative and precipitation surface fluxes assessment, correction and application on 1/4 global ocean 19892009 hindcasts, EGU General Assembly, Vienna Austria, 2011.
Gilson, J., Roemmich, D., Cornuelle, B., and Fu, L.: Relationship of TOPEX/Poseidon altimetric height to steric height and circulation in the North Pacific, J. Geophys. Res., 103, 27947–27966, 1998.
Guinehut, S., Le Traon, P.-Y., Larnicol, G., and Philipps, S.: Combining Argo and remote-sensing data to estimate the ocean three-dimensional temperature fields – A first approach based on simulated observations, J. Mar. Sys., 46, 85–98, 2004.
Guinehut, S., Le Traon, P.-Y., and Larnicol, G.: What can we learn from Global Altimetry/Hydrography comparisons ?, Geophys. Res. Lett, 33, L10604, doi:10.1029/2005GL025551, 2006.
Haines, K., Valdivieso, M., Zuo, H., and Stepanov, V. N.: Transports and budgets in a 1/4 global ocean reanalysis 19892010, Ocean Sci. Discuss., 9, 261–290, doi:10.5194/osd-9-261-2012, 2012.
Ingleby, B. and Huddleston, M.: Quality control of ocean temperature and salinity profiles - historical and real-time data, J. Mar. Sys., 65, 158–175, doi:10.1016/j.jmarsys.2005.11.019, 2007.
Larnicol, G., Guinehut, S., Rio, M.-H., Drevillon, M., Faugere, Y., and Nicolas, G.: The Global Observed Ocean Products of the French Mercator project, Proceedings of 15 Years of progress in Radar Altimetry Symposium, ESA Special Publication, SP-614, 2006.
Le Traon, P.-Y., Nadal, F., and Ducet, N.: An improved mapping method of multisatellite altimeter data, J. Atmos. Ocean. Technol., 15, 522–534, 1998.
Lherminier, P., Mercier, H., Gourcuff, C., Alvarez, M., Bacon, S., and Kermabon, C.: Transports across the 2002 Greenland-Portugal OVIDE section and comparison with 1997, J. Geophys. Res., 112, C07003, doi:10.1029/2006JC003716, 2007.
Locarnini, R. A., Mishonov, A. V., Antonov, J. I., Boyer, T. P., Garcia, H. E., Baranova, O. K., Zweng, M. M., and Johnson, D. R.: World Ocean Atlas 2009, Volume 1: Temperature, edited by: Levitus, S., NOAA Atlas NESDIS 68, US Government Printing Office, Washington, D.C.,

OSD
9, 1313–1347, 2012

184 pp., 2010.
McCarthy, M. C., Talley, L. D., and Roemmich, D: Seasonal to interannual variability from expendable bathythermograph and TOPEX/Poseidon altimeter data in the South Pacific subtropical gyre, J. Geophys. Res., 105, 19535–19550, 2000.
Meijers, A. J. S., Bindoff, N. L., and Rintoul, S. R.: Estimating the Four-Dimensional Structure of the Southern Ocean Using Satellite Altimetry, J. Atmos. Oceanic Technol., 28, 548–568, doi:10.1175/2010JTECHO790.1, 2011.
Mulet, S., Rio, M.-H., Mignot, A., Guinehut, S., and Morrow, R.: A new estimate of the global 3-D geostrophic ocean circulation based on satellite data and in situ measurements, Deep-Sea Res. Pt. II, accepted, 2012. 2012.
Oke, P. R., Balmaseda, M., Benkiran, M., Cummings, J. A., Dombrowsky, E., Fujii, Y., Guinehut, S., Larnicol, G., Le Traon, P.-Y., and Martin, M. J.: Observing System Evaluations using GODAE systems, Oceanography, 22, 144–153, 2009.
Oke, P. R., Balmaseda, M., Benkiran, M., Cummings, J. A., Dombrowsky, E., Fujii, Y., Guinehut, S., Larnicol, G., Le Traon, P.-Y., and Martin, M. J.: Observational requirements of GODAE Systems. In Proceedings of OceanObs'09: Sustained Ocean Observations and Information for Society (Vol. 2), Venice, Italy, 21-25 September 2009, Hall, J., Harrison, D. E. & Stammar, D., Eds., ESA Publication WPP-306, 2010.
Reul, N., Tenerelli, J., Chapron, B., Vandemark, D., Quilfen, Y., and Kerr, Y. H.: SMOS satellite L-band radiometer: a new capability for ocean surface remote sensing in Hurricanes, J. Geophys. Res., 117, C02006, doi:10.1029/2011JC007474, 2011.
Reynolds, R. W., Smith, T. M., Liu, C., Chelton, D. B., Casey, K. S., and Schlax, M. G.: Daily high-resolution blended analyses for sea surface temperature, J. Climate, 20, 5473–5496, 2007.
Rio, M.-H., Guinehut, S., and Larnicol, G.: New CNES-CLS09 global mean dynamic topography computed from the combination of GRACE data, altimetry, and in situ measurements, J. Geophys. Res., 116, C07018, doi:10.1029/2010JC006505, 2011.
Roemmich, D. and Gilson, J.: The 2004–2008 mean and annual cycle of temperature, salinity and steric height in the global ocean from the Argo program, Prog. Oceanogr. 82, 81–100, 2009.
Roemmich, D., Johnson, G. C., Riser, S., Davis, R., Gilson, J., Brechner Owens, W., Garzoli, S. L., Schmid, C., and Ignaszewski, M.: The Argo Program: Observing the global oceans with profiling floats. Oceanography, 22, 24–33, 2009.

OSD
9, 1313–1347, 2012

Stammer, D., Köhl, A., Awaji, T., Balmaseda, M., Behringer, D., Carton, J., Ferry, N., Fischer, A., Fukumori, I., Giese, B., Haines, K., Harrison, E., Heimbach, P., Kamachi, M., Keppenne, C., Lee, T., Masina, S., Menemenlis, D., Ponte, R., Remy, E., Rienecker, M., Rosati, A., Schrëoter, J., Smith, D., Weaver, A., Wunsch, C., and Xue, Y.: Ocean Information Provided through Ensemble Ocean Syntheses, in: Proceedings of OceanObs'09: Sustained Ocean Observations and Information for Society, edited by: Hall, J., Harrison, D. E., and Stammer, D., Vol. 2, Venice, Italy, 21–25 September 2009, ESA Publication WPP-306, 2010.

Storto, A., Russo, I., and Masina, S.: Interannual response of global ocean hindcasts to a satellite-based correction of precipitation fluxes, Ocean Sci. Discuss., 9, 611–648, doi:10.5194/osd-9-911-2012, submitted in the present MyOcean Special Issue, 2012.

Swart, S., Speich, S., Ansorge, I. J., and Lutjeharms, J. R. E.: An altimetry-based gravest empirical mode south of Africa: 1. Development and validation, J. Geophys. Res., 115, C03002, doi:10.1029/2009JC005299, 2010.

Von Schuckmann, K., Gaillard, F., and Le Traon, P.-Y.: Global hydrographic variability patterns during 2003–2008, J. Geophys. Res., 114, C09007, doi:10.1029/2008JC005237, 2009.

Willis, J. K., Roemmich, D., and Cornuelle, B.: Combining altimetric height with broadscale profile data to estimate steric height, heat storage, subsurface temperature, and sea-surface temperature, J. Geophys. Res., 108, 3292, doi:10.1029/2002JC001755, 2003.

OSD

9, 1313–1347, 2012

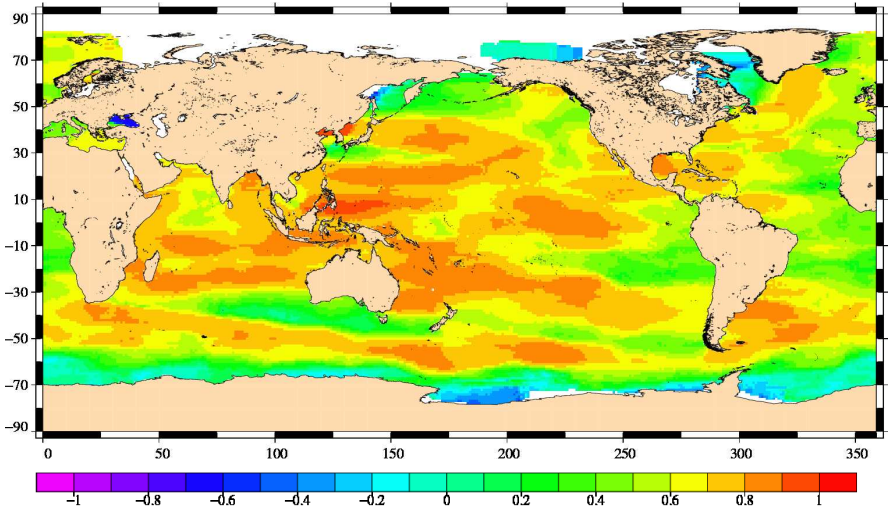

Fig. 1. Annual correlation coefficient between dynamic heights (DH) computed using a reference level at 1500 meter depth and temperature (T) field at 100 meter depth. The color scale ranges from −1 to 1, every 0.1.

OSD
9, 1313–1347, 2012

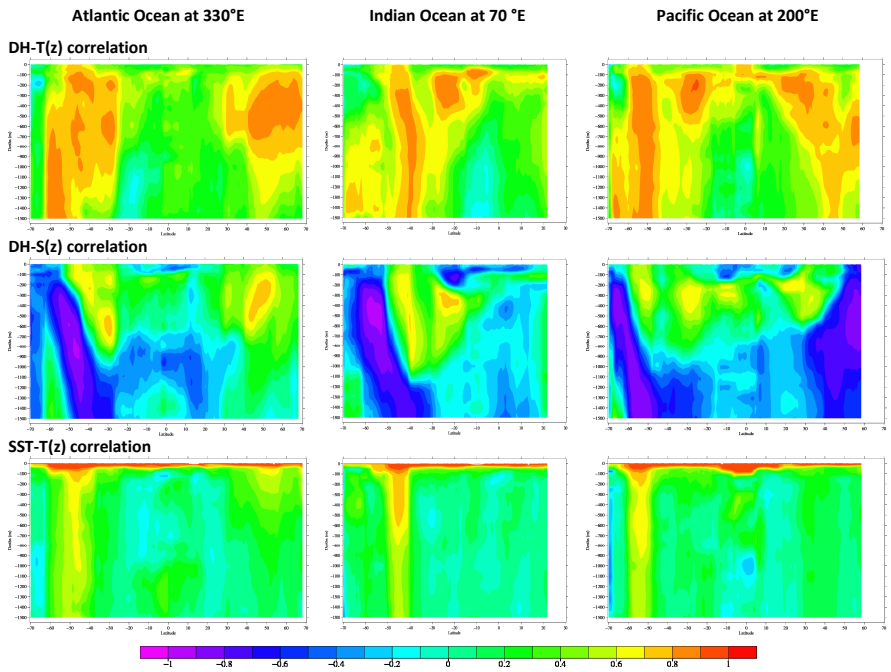

Fig. 2. DH-T(z), DH-S(z) and SST-T(z) annual correlation coefficients for three zonal sections: at 330° W in the Atlantic Ocean, at 70° W in the Indian Ocean and at 200° W in the Pacific Ocean. The latitudes range from 70° S to 70° N for the Atlantic and Pacific Oceans and from 70° S to 30° N for the Indian Ocean and the depths from 0 to −1500 m. The color scale ranges from −1 to 1, every 0.1.

OSD
9, 1313–1347, 2012

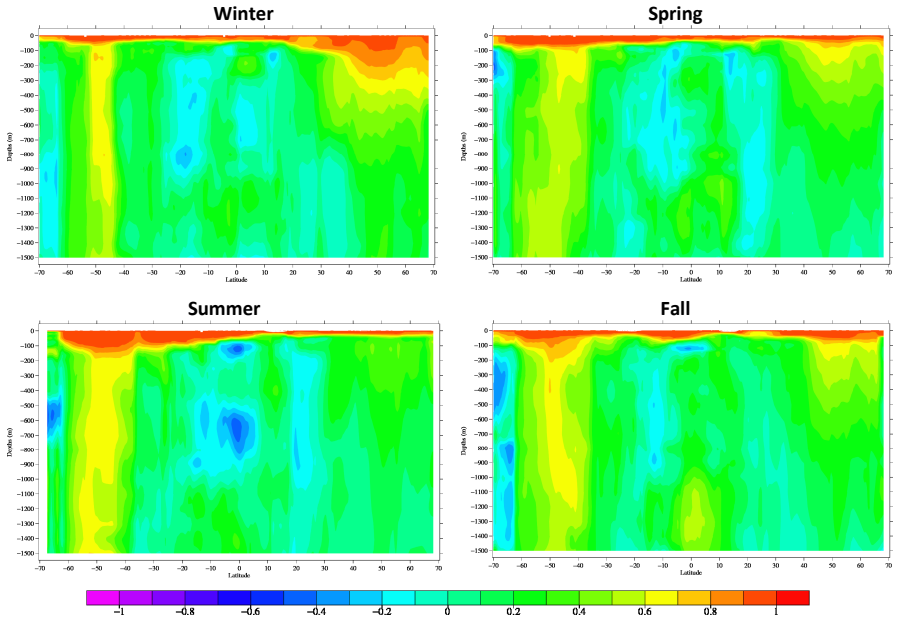

Fig. 3. SST-$T(z)$ correlation coefficients for the Atlantic Ocean zonal section at 330° W and for each season. Winter corresponds to Jan/Feb/Mar and so on.

OSD
9, 1313–1347, 2012

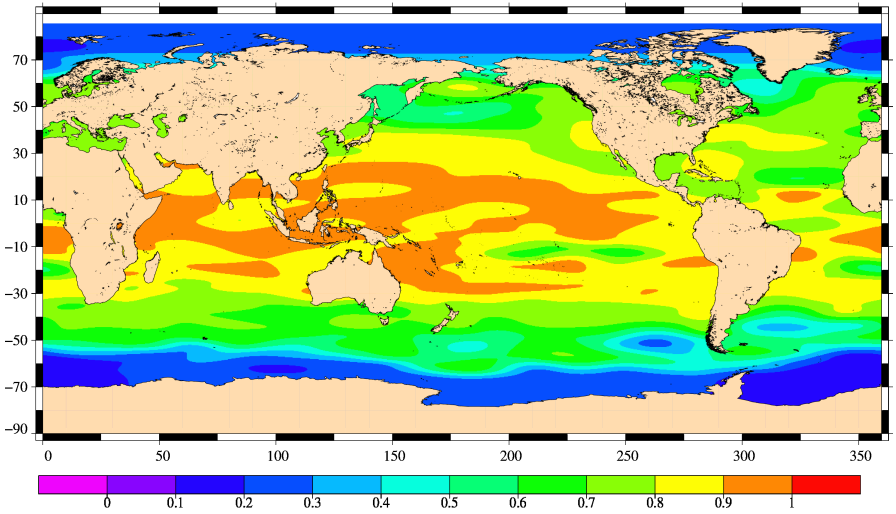

Fig. 4. Regression coefficient between SLA and DHA computed using a 1500 m depth reference level.

OSD
9, 1313–1347, 2012

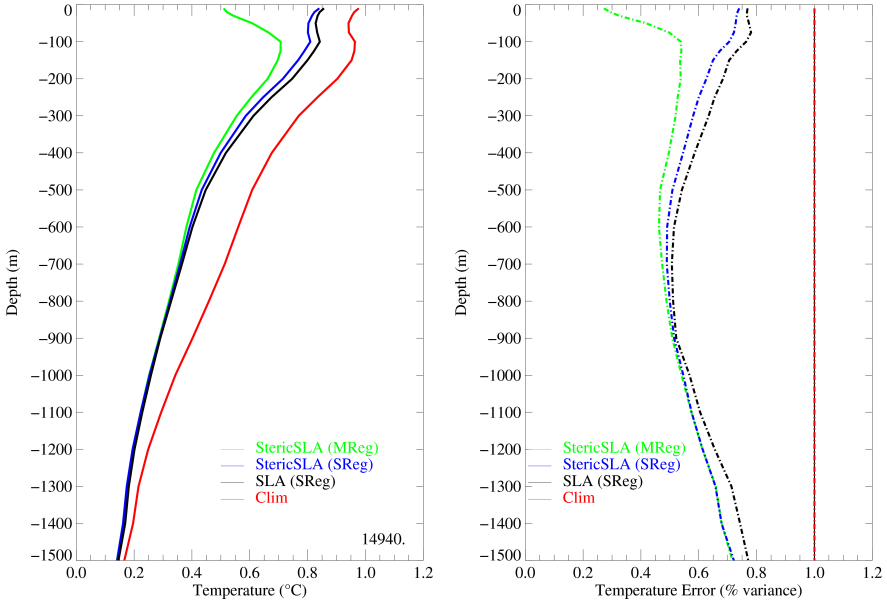

Fig. 5. Rms error in reconstructing subsurface temperature using the ARIVO monthly climatology (red) and the synthetic fields: using a simple regression method of total (black) and steric (blue) SLA and using a multiple linear regression method of steric SLA and SST (green). Rms error as percentage of signal variance (calculated from the ARIVO climatology) is also showed on right figure. 14 900 independent *T* profiles of the year 2009 and located in the ACC have been used for comparison.

OSD
9, 1313–1347, 2012

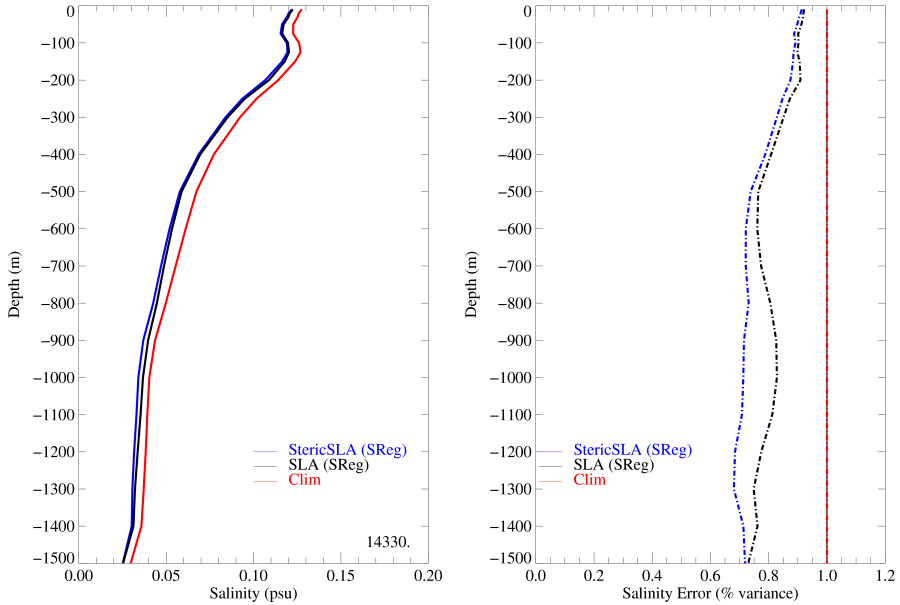

Fig. 6. Same as Fig. 5 but for subsurface salinity. 14 300 independent S profiles of the year 2009 have been used for comparison.

OSD
9, 1313–1347, 2012

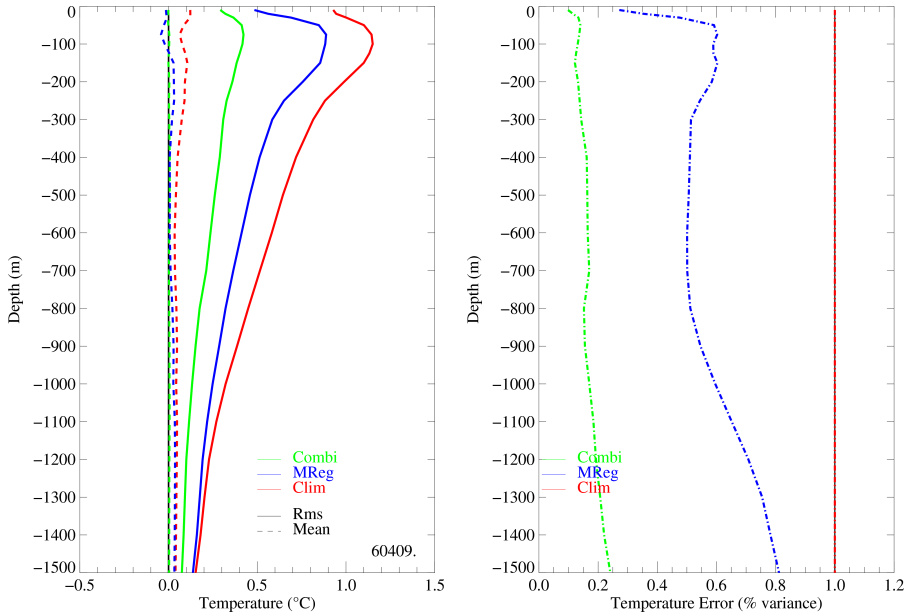

Fig. 7. Mean (dotted line) and rms error in reconstructing subsurface T using the ARIVO monthly climatology (red), the synthetic fields (blue) and the combined fields (green). Rms error as percentage of signal variance (calculated from the ARIVO climatology) are also showed on right figure. 60 400 independent T profiles of the year 2009 have been used for comparison.

OSD
9, 1313–1347, 2012

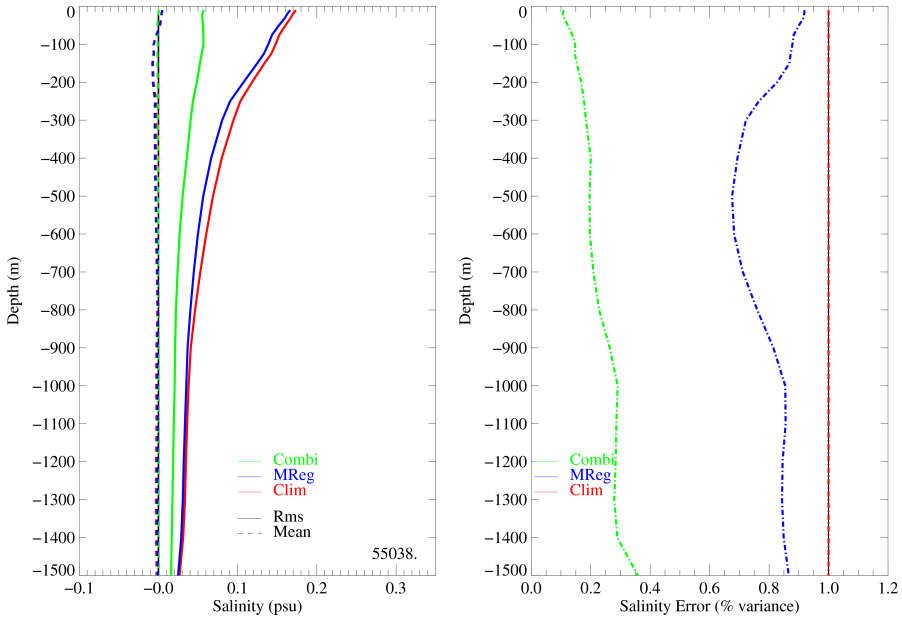

Fig. 8. Same as Fig. 7 but for subsurface S. 55 000 independent S profiles of the year 2009 have been used for comparison.

OSD
9, 1313–1347, 2012

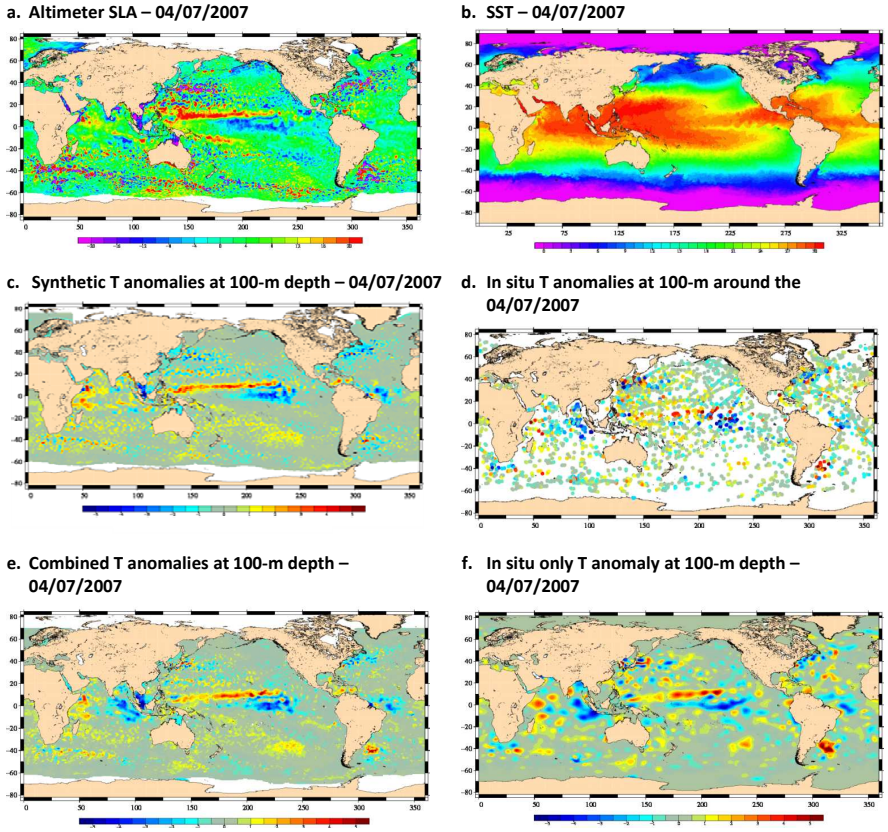

Fig. 9. Input and outputs from the GOOP system for the 4 July 2007: **(a)** altimeter SLA (in cm), **(b)** SST (in ˚C), **(c)** synthetic T anomalies at 100 m (in ˚C), **(d)** individual in situ T observations at 100 m (in ˚C), **(e)** combined T anomalies at 100 m (in ˚C). An in situ only solution for the T anomaly at 100 m is also displayed in **(f)**. (in cm).

OSD
9, 1313–1347, 2012

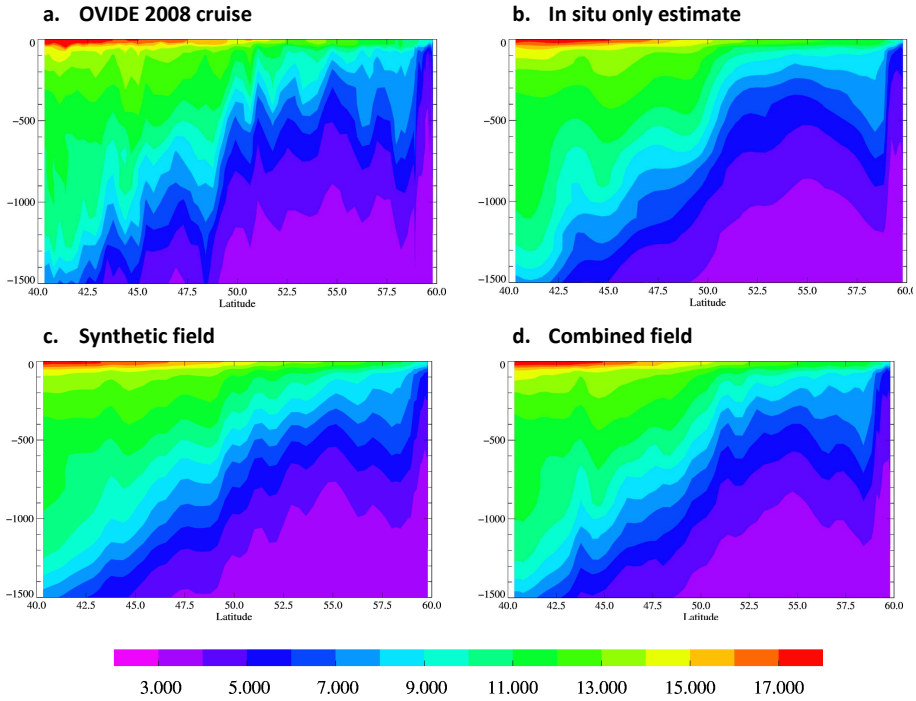

Fig. 10. Temperature field from **(a)** the OVIDE 2008 section, **(b)** an in situ only estimate, **(c)** the synthetic fields and **(d)** the combined fields (in ˚C). Note that observations from the OVIDE section have not been used to compute the in situ only estimate and the combined estimate.

OSD
9, 1313–1347, 2012

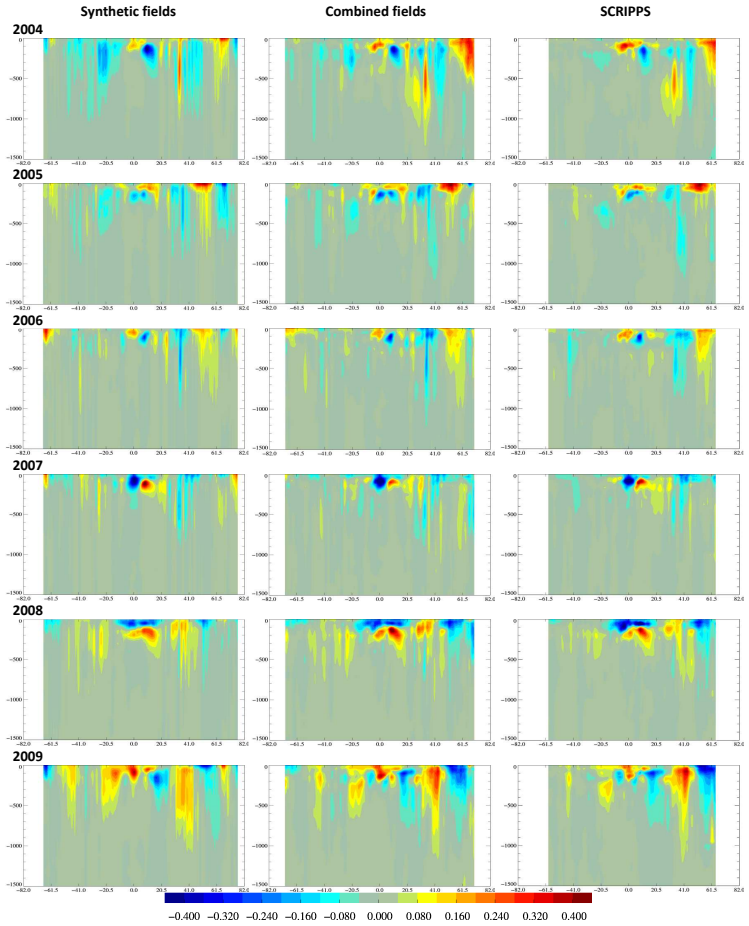

Fig. 11. Yearly zonal averages of the synthetic, combined and SCRIPPS temperatures as anomalies from the 2004 to 2009 periods (in °C). The latitudinal extent of each fields are slightly different.

OSD
9, 1313–1347, 2012

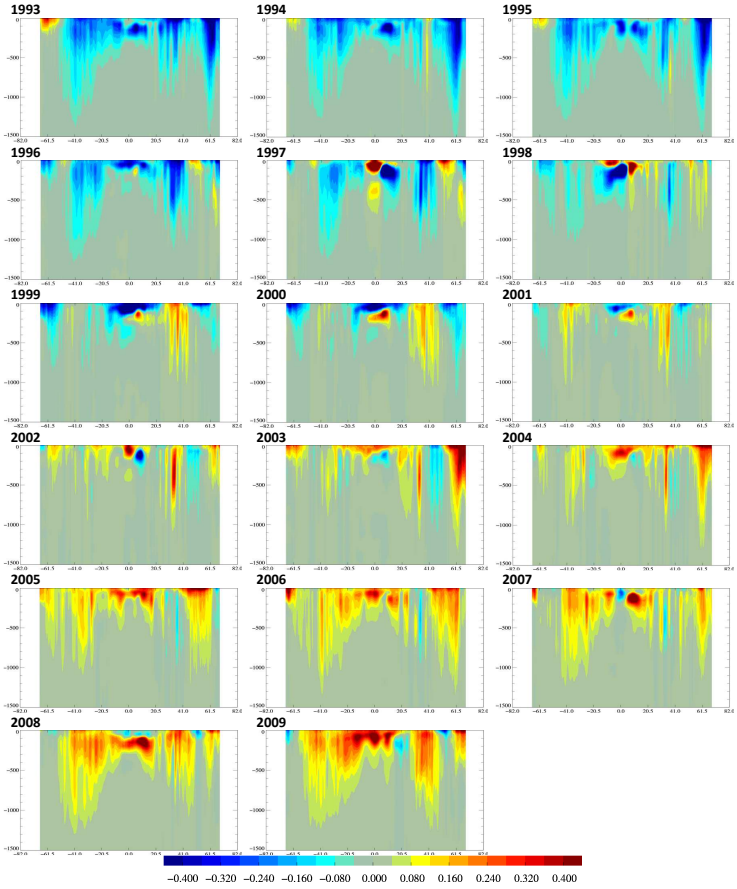

Fig. 12. Yearly zonal averages of the combined temperatures as anomalies from the 1993 to 2009 periods (in ˚C).

OSD
9, 1313–1347, 2012